

In-Situ Determination of Powder-Laser Focus Overlap in High-Speed DED Using Multispectral Emission Analysis

Patrick Gajek*; Helena Wexel*, Frederik Zanger*

*wbk Institute of Production Science, Karlsruhe Institute of Technology (KIT),
Kaiserstr. 12, 76131 Karlsruhe, Germany

Abstract

Precise spatial alignment between the laser and powder focus is critical for achieving complete particle melting and stable process conditions in high-speed Directed Energy Deposition (HS-DED). This work presents an in-situ diagnostic approach using a photometric emission sensor to identify and calibrate the spatial overlap of laser and powder focus during the deposition of AISI 316L. During the incremental translation of the powder nozzle towards the laser focal point, spectral emission data are recorded and subsequently correlated with the local photometric intensity and the corresponding spectral temperature distribution. A distinct emission maximum and consistent spectral shift are observed when the powder focus coincides with the laser focus, indicating optimal energy absorption and melting behavior. This method allows precise focus alignment without invasive measurements, improving reproducibility and deposition quality. The approach presented supports process monitoring and control related high-speed DED systems, and is broadly transferable across materials and system configurations.

1. Introduction

High-Speed Directed Energy Deposition (HS-DED) is increasingly gaining importance as an Additive Manufacturing (AM) process for the repair, coating and production of near-net-shape metallic components. In contrast to powder bed-based AM processes, DED enables significantly higher deposition rates and flexible material combinations. Among these technologies, HS-DED stands out due to its potential to reach deposition speeds beyond 200 m/min while maintaining high geometric fidelity and thermal control [1].

The fundamental enabler of this process performance lies in the positioning of the powder focus above the workpiece surface, allowing particles to melt in-flight prior to reaching the substrate. This concept reduces interaction time between powder and melt pool, thus enabling ultra-fast buildup with tailored thermal gradients [2,3]. This advantage introduces new challenges: the powder-laser interaction becomes highly sensitive to positional mismatches, and small deviations between powder and laser focus can lead to incomplete particle melting, excessive spatter formation, or unstable melt pool dynamics [4].

In current industrial systems, the alignment of powder and laser focus is often performed manually or semi-empirically and lacks real-time feedback. Conventional optical methods like triangulation or coaxial imaging have limited resolution or are incompatible with the dynamic nature and compact working zones of HS-DED [5,6]. Therefore, a robust and high-speed compatible in-situ monitoring method that can detect and quantify the effective overlap between powder and laser beam is of high interest for industrial adoption.

A promising approach lies in the use of spectral emission analysis, which can reveal characteristic features of the laser-powder interaction zone. The thermal radiation emitted by the melt pool and interacting particles carries information about local energy absorption, temperature distribution, and dynamic behavior. Multispectral sensors such as the 4D.Two (4D Photonics GmbH) offer combined detection of visible and near-infrared signals with high temporal resolution (>1 MS/s), enabling process analysis in real time. In addition, physical models of the interaction process, as established for DED processes, show that specific emission peaks and spectral shifts

correspond directly to the onset of full particle melting and stable process zones [3]. These relationships offer a pathway to a non-invasive and quantitative method for focus calibration.

This study investigates such an approach using the 4D. Two multispectral sensor for in-situ determination of the powder-laser overlap. By systematically shifting the powder nozzle relative to the fixed laser focus in X and Y directions, we analyze the corresponding changes in spectral emission behavior during the deposition of AISI 316L. The aim is to identify the spatial position of optimal overlap – indicated by peak emission intensity and stable thermal signature – and to demonstrate a diagnostic method that supports precision alignment and robust process control in HS-DED systems.

2. Multispectral Analysis and Methods

The experimental setup, as shown in Figure 1, is based on a PE3D system (Ponticon GmbH, Wiesbaden, Germany), which supports two operation modes: a 3-axis and a 5-axis configuration. For the present study, the 3-axis mode was used, in which the build platform can move in the X, Y, and Z directions while the processing head remains stationary. The system includes a cylindrical build volume of 700 mm × 600 mm and supports high dynamic motion with deposition speeds up to 200 m/min and accelerations of up to 5 g. The positioning system offers a path accuracy of 0.03 mm.

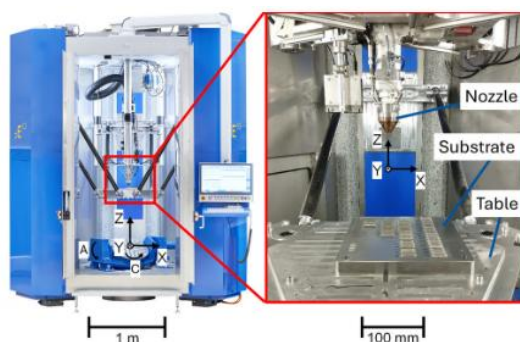


Fig. 1. Ponticon experimental setup

The laser source is an LDF 6000-40 diode laser (Laserline GmbH, Mülheim-Kärlich, Germany) with a fiber core diameter of 400 μm and a maximum output power of 6 kW. Together with a Laserline process head, the system enables a defined top-hat intensity distribution and focus spot diameters between 1.0 mm and 3.2 mm. The powder is supplied coaxially through a continuous annular gap nozzle (BLC Laserschneidtechnik GmbH, Bad Marienberg, Germany), which delivers the powder flow centrally into the laser beam. The nozzle lateral adjustment in the X and Y directions with respect to the laser focal axis.

As material, gas-atomized AISI 316L stainless steel powder with a particle size distribution of 20–63 μm (m4p material solutions GmbH, Magdeburg, Germany) was used. The powder was deposited on a cold-rolled 1.0038 mild steel substrate.

A coaxial powder nozzle from Laserline GmbH was employed to generate a stable and symmetrical powder–gas stream into the laser interaction zone. The nozzle features a conical annular geometry formed by an inner and outer cone, through which the powder–gas mixture is guided, as shown in figure 2.

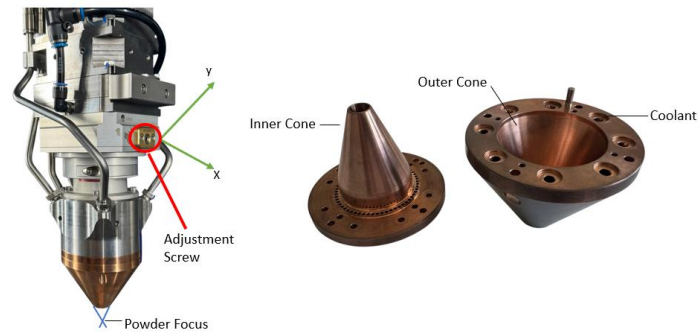


Fig. 2. Powder nozzle assembly (left: HS-DED nozzle system; right: disassembled powder nozzle)

Particles are redirected along the inner conical surface and focused toward the nozzle tip, generating a hollow conical jet that converges into a well-defined powder focus. This design enables consistent material delivery an essential requirement for stable laser–particle interaction at high deposition speeds. This nozzle comes with an integrated adjustment mechanism, which allows for lateral displacement of the powder stream in the X and Y directions. This is accomplished via an internal fine-threaded screw that shifts a mounting plate, enabling precise tuning of the powder–laser overlap without altering the external alignment of the nozzle or affecting the optical path.

To systematically investigate the impact of lateral misalignment, the powder stream position was varied in defined steps while the laser focal plane in Z-direction remained fixed at a working distance of 13 mm. A total of 21 single-track welds were deposited under controlled process conditions. Ten sets of tracks introduced X-offsets ranging from -0.5 mm to $+0.5$ mm in 0.1 mm increments, followed by ten sets of tracks with equivalent Y-offsets, as shown in table 1.

Table 1. Test plan for systematic evaluation of laser-powder focus alignment via x and y offset

| Parameter Set | P_L in W | Δx in mm | Δy in mm | Parameter Set | P_L in W | Δx in mm | Δy in mm |
|---------------|------------|------------------|------------------|---------------|------------|------------------|------------------|
| V 5.0 | 2000 | 0.0 | 0.0 | V 5.11 | 2000 | 0.0 | 0.1 |
| V 5.1 | 2000 | 0.1 | 0.0 | V 5.12 | 2000 | 0.0 | 0.2 |
| V 5.2 | 2000 | 0.2 | 0.0 | V 5.13 | 2000 | 0.0 | 0.3 |
| V 5.3 | 2000 | 0.3 | 0.0 | V 5.14 | 2000 | 0.0 | 0.4 |
| V 5.4 | 2000 | 0.4 | 0.0 | V 5.15 | 2000 | 0.0 | 0.5 |
| V 5.5 | 2000 | 0.5 | 0.0 | V 5.16 | 2000 | 0.0 | -0.1 |
| V 5.6 | 2000 | -0.1 | 0.0 | V 5.17 | 2000 | 0.0 | -0.2 |
| V 5.7 | 2000 | -0.2 | 0.0 | V 5.18 | 2000 | 0.0 | -0.3 |
| V 5.8 | 2000 | -0.3 | 0.0 | V 5.19 | 2000 | 0.0 | -0.4 |
| V 5.9 | 2000 | -0.3 | 0.0 | V 5.20 | 2000 | 0.0 | -0.5 |
| V 5.10 | 2000 | -0.4 | 0.0 | | | | |

One centrally positioned track, aligned manually based on visual observation of the powder–laser overlap, served as the reference condition for all spectral comparisons. All experiments, constant parameters were maintained to ensure reproducibility and isolate the effects of lateral offset. These included a laser power of 2000 W, a traverse speed of 30 m/min, a shielding gas flow of 14 l/min, and a track length of 20 mm. This stable process environment enabled a focused analysis of how lateral misalignment influences spectral emission

characteristics observed via multispectral sensing. To monitor the laser–powder interaction zone during the DED process, a 4D.Two multispectral sensor (4D Photonics GmbH) was mounted externally to the process chamber, while its optical interface was integrated coaxially into the beam path. This configuration enables real-time, coaxial observation of the melt pool and powder-laser overlap, ensuring that the emitted radiation is captured along the same optical axis as the laser, without obstructing the powder or energy flow. The setup provides an undistorted and accurate view of the interaction region during deposition. The sensor system operates with an array of photodiodes coupled to high-speed capacitor-based signal acquisition electronics. Each photodiode converts the incoming optical signal into an analog electrical signal, which is sampled at rates exceeding one million samples per second. The signals are buffered in fast-response capacitors, then digitized and stored in a synchronized SQLite database. A hardware trigger linked to the process start ensures precise temporal alignment of the recorded signals with the onset of laser activity.

The channel assignment is predefined: visible (VIS) channels correspond to internal IDs 16–31, and near-infrared (NIR) channels to IDs 48–63. Each channel is mapped to a specific central wavelength through the 4D.lab software, and this mapping remains constant during operation. The system records data continuously over time, with each row representing a time step and each column a spectral channel. This configuration enables high-resolution, multispectral analysis of emission dynamics related to melting, heating, and energy coupling in the laser–powder interaction zone.

The HS-DED process is governed by a complex physical interaction between a high-power laser beam and a stream of material that is simultaneously delivered to the substrate. The laser energy melts both the feedstock material and the surface of the substrate, generating a localized melt pool that solidifies rapidly to form a metallurgical bond and build up the part layer by layer [7,8]. The interaction mechanism depends on several parameters, including laser power, focus position, scanning speed, and powder feed rate, which together determine the thermal input, melt pool dynamics, and the efficiency of material consolidation [9–11]. In HS-DED, the powder is injected into the laser interaction zone via a coaxial or lateral nozzle. The motion of the particles, typically influenced by gravity and the flow of carrier gas, follows ballistic trajectories. Their distribution and velocity depend on the volumetric flow rate of the carrier gas V , the annular nozzle gap r_0 and the nozzle exit radius r . The particle velocity v_p can be estimated via the simplified expression

$$v_p = \frac{V}{4\pi r r_0}, \quad \text{Eq.1}$$

which is critical for modeling the interaction zone and understanding the particle residence time within the laser beam [19,20]. The formation and stability of the melt pool are closely linked to the laser–material coupling efficiency, which itself is modulated by the spatial overlap of the laser focus and the powder stream. During their flight, powder particles absorb part of the laser energy before reaching the substrate, the melting process begins mid-flight. The laser radiation is absorbed both by flying particles and by the melt pool surface, with additional heat transferred to the substrate through conduction. This multistage interaction enhances energy efficiency and allows higher build rates [3]. The effectiveness of this energy coupling is highly sensitive to the particle size, velocity, and beam focus configuration. The presence of powder in the beam path introduces powder-induced attenuation, a critical factor affecting the energy input to the substrate. When the laser beam intersects the powder stream, a portion of the beam is absorbed or scattered by the particles. This reduces the net power reaching the substrate and modifies the melt pool geometry [12,13]. The degree of attenuation depends on powder concentration, particle size distribution, and the spatial distribution of the powder stream [14,15]. In highly concentrated powder streams, attenuation becomes significant, reducing laser penetration and thus limiting energy availability at the substrate surface. This attenuation effect can be quantified through integrative models. For example, the average attenuated power P_d in relation to the initial laser power P can be expressed as:

$$\frac{P_d}{P} = \frac{3}{4r_m^3} \times \iiint r^2 \times \left(1 - \frac{v_{pz}}{v_{py}}\right)^2 \times dx \, dy \, dr, \quad \text{Eq.2}$$

where r_m denotes the mean particle radius, v_{pz} the axial velocity component, and v_{py} the radial velocity component of the particles. This model accounts for the scattering cross-section and transit geometry of the powder cloud [20]. A key parameter in the process control is the spatial overlap between the laser focus and the powder focal point, which critically influences the thermal history of the particles. Only when the focal zones are well aligned the particles absorb enough energy during flight to ensure complete melting before deposition. Misalignment - whether axial or radial - can lead to insufficient particle heating, partial melting, or even unmelted inclusions in the final build [16,17]. Such defects reduce layer adhesion and can compromise the mechanical properties of the component. Therefore, optimizing this overlap is essential to maximize energy coupling, stabilize the melt pool, and enhance the powder catchment efficiency

$$\eta = \frac{A_m}{A_p}, \quad \text{Eq.3}$$

which defines the ratio of melt pool area A_m to the projected area of the powder stream A_p . As noted by Schopphoven et al. [3], a concentric alignment of the laser and powder focus achieves the highest absorption efficiency per unit of powder mass, while asymmetric focusing results in uneven thermal gradients, spatter formation, and inhomogeneous microstructures. Furthermore, accurately determining the melt pool size and its correlation with the powder flux is crucial for predictive process modeling [20]

The observed radiation is a superposition of multiple emission mechanisms, predominantly: Thermal emission (continuous spectrum) from the melt pool and heated particles, line emission (discrete spectrum) originating from atomic transitions in excited species (atoms, ions), reflected or scattered laser radiation, and plasma-induced continuum radiation, in high-energy regimes.

The thermal emission from a hot surface can be described by the Planck radiation law, which defines the spectral radiance $I(\lambda, T)$ as a function of the wavelength λ and the temperature T of the emitter:

$$I(\lambda, T) = \frac{2\pi hc^2}{\lambda^5} \times \frac{1}{e^{\frac{hc}{\lambda kT}} - 1}. \quad \text{Eq.4}$$

This function describes the spectral distribution of an ideal blackbody radiator, which exhibits a peak emission at a specific wavelength depending on its temperature. The displacement of this peak toward shorter wavelengths with increasing temperature is described by Wien's displacement law:

$$\lambda_{max} = \frac{b}{T}. \quad \text{Eq.5}$$

These fundamental relations form the basis of pyrometric measurement using optical sensors [26]. Since materials deviate from ideal blackbody behavior, a material-specific emissivity $\varepsilon(\lambda)$ must be considered. The actual spectral radiance of a real material is therefore given by:

$$I_{real}(\lambda, T) = \varepsilon(\lambda) \times I_{blackbody}(\lambda, T). \quad \text{Eq.6}$$

The emissivity depends on surface condition, oxidation layer, alloy composition, and observation angle. Consequently, accurate temperature measurement and interpretation of spectral signals require either knowledge or estimation of the material's emissivity [26]. In high-power laser applications and particularly in focused processes, the intense energy input can cause partial vaporization and ionization of the material, resulting in the formation of a plasma plume above the melt pool. This plasma emits radiation due to electronic transitions of atoms and ions, which produces sharp and element-specific spectral lines [27]. Such emissions are governed by the principles of atomic emission spectroscopy. The intensity I_i of a spectral line associated with a transition from an upper energy level i to a lower level j is given by:

$$I_{ij} \propto N_i \times A_{ij} \times h\nu. \quad \text{Eq.7}$$

In this expression, N_i denotes the population of the upper energy state, A_{ij} is the Einstein coefficient for spontaneous emission for the corresponding transition, and $h\nu$ represents the photon energy of the emitted light. The population of the upper level N_i is determined by the Boltzmann distribution, which introduces a direct temperature dependency into the emission intensity. As a result, the presence and strength of specific spectral lines can not only be used to identify chemical elements but also to estimate the excitation temperature of the plasma under the assumption of local thermodynamic equilibrium [26]. The optical spectrum emitted during the HS-DED process carries a wealth of multidimensional information about the state of the process. The overall spectral shape of the continuum emission primarily reflects the temperature of the surface or melt pool, providing insight into thermal conditions. In addition, the presence and intensity of discrete spectral lines indicate the elemental composition of the vaporized material, enabling chemical analysis of the interaction zone. Changes in line width, particularly those caused by broadening, offer a means to estimate the density of the plasma formed above the melt pool. Furthermore, temporal fluctuations in the spectral signal are closely linked to dynamic events in the process such as spattering, keyholing, or lack of fusion, and can therefore serve as indicators of stability or anomalies within the deposition sequence [26].

To quantify this behavior, a sensitivity score was computed for each channel by averaging its deviation from the reference track across all runs with defined lateral offsets. Separate sensitivity profiles were calculated for the X- and Y-directions based on the corresponding groups of runs. This analysis revealed how strongly each channel responded to a given directional misalignment and enabled selection of the three most sensitive channels per axis for detailed focus optimization.

For these selected channels, a polynomial curve fitting approach was applied. Deviation values were plotted against the known physical offset positions, and a second-degree polynomial (parabola) was fitted to the data. The minimum of each fitted parabola—calculated analytically—was interpreted as the optimal offset at which spectral similarity to the reference was highest, corresponding to optimal spatial overlap of laser and powder. This method offers an objective, data-driven alternative to conventional visual alignment techniques. In the case of Y-direction analysis, where optical centering proved inaccurate, the reference point was redefined based on morphological inspection of the weld tracks. The spectral analysis was repeated using this new reference, which resulted in symmetric parabolic deviation profiles and further validated the refined alignment. The results included time-resolved emission curves, heatmaps of channel-wise deviations, sensitivity distributions across wavelengths, and fitted deviation curves for focus optimization. This comprehensive approach enabled precise identification of spectral channels most indicative of focus quality and facilitated accurate localization of the laser-powder interaction optimum.

3. Results and Discussion

To quantitatively assess the sensitivity of the multispectral signals to lateral focus deviations, the three most responsive channels in the X-direction were selected based on the results shown previously. Figure 3 (left) illustrates the deviation of these channels from the optically defined focus point as a function of the introduced X-offset. When plotting the deviation of an individual selected channel as a function of the introduced X-offset (cf. Figure 4), a parabolic trend becomes clearly visible, confirming that the deviation behaves symmetrically around a well-defined minimum. These curves were fitted using a second-degree polynomial, and the analytical minima closely match the zero-offset position, thereby validating the accuracy of the initial visual alignment along the X-axis.

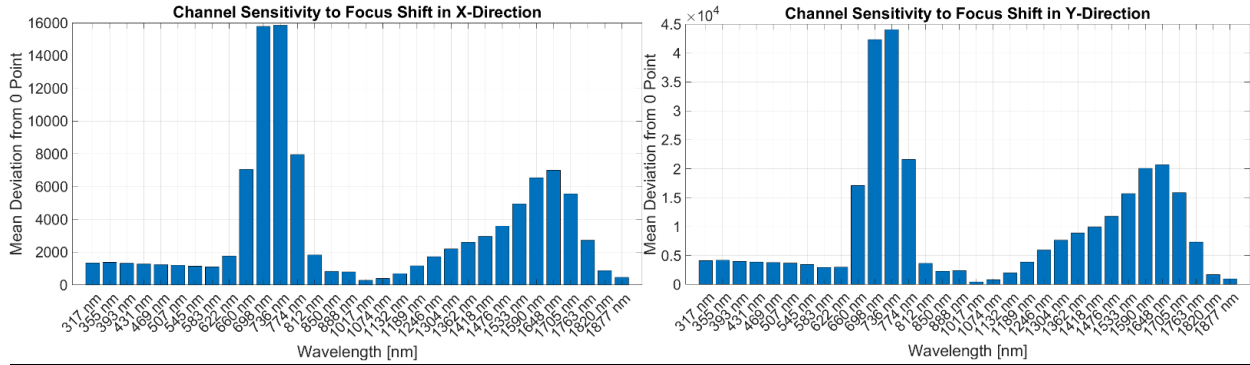


Fig. 3. Chanel sensitivity on focus shift (left: x-direction, right: y-direction)

The observed sensitivity maxima for these channels are physically plausible when considering the fundamental emission mechanisms involved. Channels located in the upper visible range (660–774 nm) and lower near-infrared region (1246–1418 nm) exhibited the strongest deviations, which can be attributed to their spectral proximity to the peak emission wavelengths for thermally excited steel surfaces. According to Planck’s radiation law (Eq. 4), the intensity of thermal radiation increases with temperature and shifts towards shorter wavelengths. For typical melt pool temperatures of 2000–3000 K, the corresponding peak emission according to Wien’s displacement law (Eq. 5) lies in the range of approximately 1000–1500 nm.

Although this spectral region contains the thermal maximum, the highest sensitivity in Figure 3 does not necessarily coincide with this peak. This discrepancy can be explained by the spectral response characteristics of the sensor, optical transmission losses, and additional emission mechanisms such as plasma continuum or line radiation. In practice, the measured signal is a convolution of thermal and non-thermal contributions. Channels with lower absolute intensity but higher signal-to-noise ratio or steeper response to local fluctuations can exhibit stronger sensitivity to defocusing. Hence, spectral sensitivity is not solely governed by peak intensity but also by how effectively a given wavelength responds to changes in energy–matter interaction dynamics.

In the context of the HS-DED process, lateral misalignment between powder stream and laser focus alters the spatial overlap and consequently the melt pool formation. As this overlap deteriorates, less energy is effectively transferred into the powder particles, reducing preheating and in-flight melting. This, in turn, lowers the melt pool temperature and diminishes thermal emission intensity, particularly in the aforementioned sensitive spectral regions. The deviation curves in Figure 3 thus capture not only the geometrical misalignment but also its direct thermophysical consequences on the emission behavior. Spectral channels in this range may also contain weak line emissions from alloying elements or oxidation products, which become more prominent when energy input is suboptimal. These additional contributions can amplify the sensitivity of specific wavelengths to small changes in local process conditions, providing a multi-faceted diagnostic signal. The choice of these wavelength bands for focus monitoring is therefore not arbitrary but rooted in both the thermodynamic emission profile of the material and the nature of energy–matter interaction in high-power laser processes.

The results in Figure 3 demonstrate that spectral analysis, particularly in carefully selected VIS/NIR regions, offers a robust and physically grounded method for detecting and quantifying focus misalignment in HS-DED. The clear parabolic behavior observed further supports the feasibility of using polynomial regression for automated alignment and control strategies. Figure 4 illustrates the results of the focus overlap optimization in X-direction based on the three most sensitive spectral channels identified from the deviation analysis: 756 nm, 768 nm, and 774 nm. For each of these channels, the absolute deviation from the reference signal—originally set via visual alignment—was calculated as a function of the applied lateral offset in X-direction. The data points were fitted using second-degree polynomials, yielding three parabolic curves with well-defined minima. The black dashed line marks the nominal zero-offset position, while the orange line highlights the visually determined reference track.

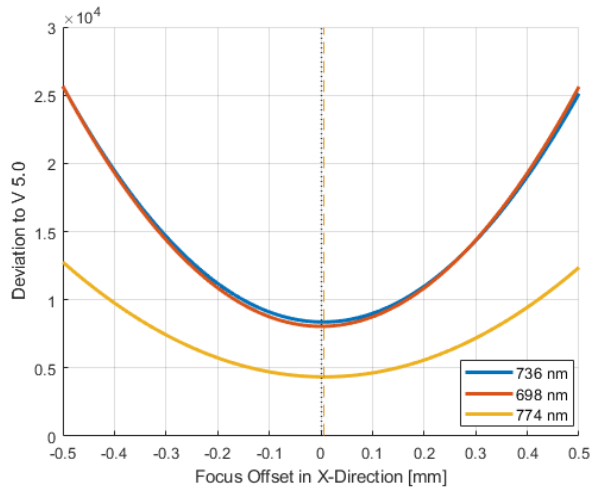


Fig. 4. Focus overlap optimization x-direction

Unlike the broader heatmap-based assessment in Figure 3, this figure focuses on a localized and wavelength-specific quantification of the overlap quality. The proximity of all three parabolic minima to zero offset confirms that the visual alignment in X-direction provided a nearly optimal spatial overlap between laser beam and powder stream. The physical rationale behind the use of these specific wavelengths lies in their high temperature sensitivity. In the upper visible spectrum, emission intensity increases rapidly with rising temperature due to the exponential nature of Planck's law (Eq. 4). As the powder–laser alignment deteriorates on either side of the focus, the reduced energy density in the melt pool leads to lower peak temperatures, which in turn reduces the radiative output at these wavelengths. Since the observed radiation in this range originates primarily from the thermal emission of the melt pool surface, small deviations in local energy input manifest as measurable intensity shifts. The parabolic shape of the deviation curves further reflects the symmetrical nature of this thermal response: energy absorption and emission efficiency decline uniformly with increasing offset, whether positive or negative. This behavior is consistent with theoretical expectations based on the melt pool's sensitivity to spatial energy distribution and supports the use of this analytical model for alignment purposes. The spectral deviation analysis for the Y-axis, illustrated in Figure 5, reveals that the fitted minima of the deviation curves for the three most sensitive channels (698 nm, 738 nm, and 774 nm) are clearly shifted away from the optical center (V 5.0).

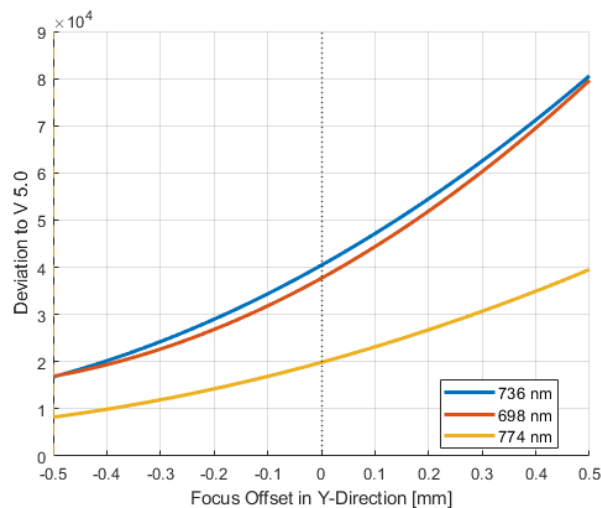


Fig. 5. Estimated optimal focus alignment y-direction

This suggests that the initial visual alignment did not coincide with the actual point of maximum energy coupling in the Y-direction. Unlike the X-axis, where the parabolic fits exhibited minima near zero offset (Figure 4), the Y-axis response lacked symmetry (V 5.15), indicating that the laser-powder overlap was not centered as presumed. This asymmetry is further supported by the macroscopic morphology of the weld seams shown in Figure 6. Each of the 21 weld beads corresponds to a defined lateral offset, and their visual appearance varies significantly. The weld tracks at offsets V5.15 and V5.12, highlighted by green arrows in Figure 6, are particularly emphasized, as they illustrate the contrast between an asymmetric and a more stable overlap condition.

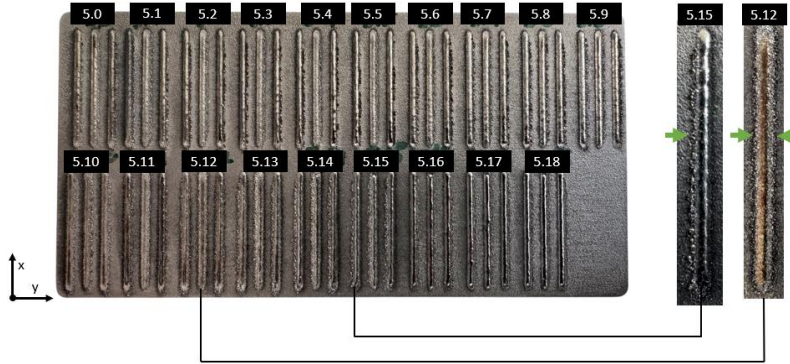


Fig. 6. Substrate with single welds

Notably, the bead corresponding to a Y-offset of +0.2 mm (V 5.12) shows the most uniform width and minimal spatter. These features suggest optimized melt pool stability and efficient powder catchment-key indicators of proper energy coupling. The presence of asymmetric spatter and irregular bead geometry in adjacent tracks highlights the sensitivity of the process to focus alignment. Such morphological deviations stem from localized variations in heat input and melt pool dynamics, which are in turn governed by the spatial overlap of laser intensity and powder distribution.

Given these observations, the reference point for the spectral analysis was redefined at V 5.12, and the deviation analysis was repeated. The recalculated results are depicted in Figure 7. Here, the parabolic fits for the same sensitive channels now exhibit well-centered, symmetric profiles around the new zero position.

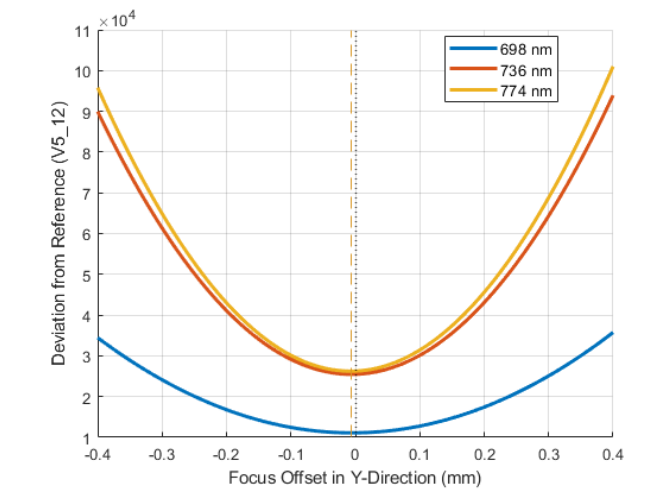


Fig. 7. Focus overlap optimization y-direction

This confirms that the updated reference accurately reflects the true optical overlap and validates the diagnostic capability of the multispectral system.

The observed spectral deviations can be attributed to fundamental effects of thermal radiation and energy coupling in the laser-powder interaction zone. Lateral misalignment alters the spatial distribution of laser intensity across the powder stream, leading to asymmetric heating, uneven melt pool formation, and changes in emissivity. These shifts affect both the thermal continuum and line emission, resulting in wavelength-dependent signal variations captured by the multispectral sensor. The parabolic deviation profiles across offset positions reflect this sensitivity and align with physical models such as Planck's and Boltzmann's laws. After redefining the reference in Y-direction based on weld morphology, the spectral minima aligned symmetrically with the new center, confirming that multispectral emission analysis enables sub-millimeter accurate detection of optimal focus positions. This method surpasses visual alignment in precision and provides a physically grounded, non-intrusive tool for enhancing process control and deposition quality in HS-DED applications.

4. Conclusion and Outlook

This work presents a comprehensive methodology for identifying and optimizing the laser-powder interaction zone in HS-DED processes using multispectral emission analysis. By systematically evaluating spectral deviations across both the visible (VIS) and near-infrared (NIR) regions, we demonstrate that lateral misalignment in beam focus can be quantitatively assessed. The proposed sensitivity-based analysis allows the identification of channels most responsive to defocus, which were subsequently used to estimate optimal focal positions in both X and Y directions.

A key finding of this study is that the optically chosen focus position, while seemingly centered, did not coincide with the thermally optimal interaction point-particularly in the Y-direction. Through correlation of spectral data with visual weld morphology (Figure 6), a new reference point was introduced, improving the symmetry and stability of the derived sensitivity profiles. The results confirm that deviations in beam-powder overlap manifest clearly in the emission signal and that these deviations follow physically plausible trends, consistent with fundamental radiative and thermal behavior. Overall, the presented approach provides a robust basis for real-time monitoring and optimization of laser-powder interactions, with potential for broad applicability across laser-based Additive Manufacturing processes. While the current study validates the feasibility of using spectral deviations to detect and quantify focus misalignments, it also highlights the limitations of manual setup and calibration. The current method relies on predefined tracks and manual alignment of the nozzle relative to the laser beam, which is both time-consuming and prone to operator error. To fully exploit the potential of spectral feedback for process stability and quality control, future work will focus on integrating the method into a closed-loop control system. This includes the development of a real-time feedback and regulation strategy based on multispectral sensor data. Such a system would continuously monitor spectral deviations and autonomously adjust the relative positioning of the powder and laser, eliminating the need for manual intervention and ensuring consistent process quality.

In this context, the results of this study serve as an important proof of concept, demonstrating that spectral analysis is not only sensitive to focus variations, but also suitable as a foundation for intelligent, sensor-driven process control in Additive Manufacturing.

5. Acknowledgements

This research and development project is funded by the German Federal Ministry of Research, Technology and Space (BMFTR) within the program "The Future of Value Creation – Research on Production, Services and Work" (funding number: 02J23C101) and managed by the Project Management Agency Karlsruhe (PTKA). The authors are responsible for the content of this publication.

References

- [1] J. Schaible, L. Sayk, T. Schopphoven, J.H. Schleifenbaum, C. Häfner, Development of a high-speed laser material deposition process for Additive Manufacturing, *J. Laser Appl.* 33 (2020) 012021. <https://doi.org/10.2351/7.0000320>.
- [2] X. Lin, K. Zhu, J.Y.H. Fuh, X. Duan, Metal-based Additive Manufacturing condition monitoring methods: From measurement to control, *ISA Trans.* 120 (2022) 147–166. <https://doi.org/10.1016/j.isatra.2021.03.001>.
- [3] T. Schopphoven, Experimental and Model-theoretical Investigations on Extreme High-speed Laser Material Deposition, RWTH Aachen University, 2020.
- [4] S. Donadello, M. Motta, A.G. Demir, B. Previtali, Monitoring of laser metal deposition height by means of coaxial laser triangulation, *Opt. Lasers Eng.* 112 (2019) 136–144. <https://doi.org/10.1016/j.optlaseng.2018.09.012>.
- [5] S. Donadello, V. Furlan, A.G. Demir, B. Previtali, Interplay between powder catchment efficiency and layer height in self-stabilized laser metal deposition, *Opt. Lasers Eng.* 149 (2022) 106817. <https://doi.org/10.1016/j.optlaseng.2021.106817>.
- [6] S. Maffia, V. Furlan, B. Previtali, Coaxial and synchronous monitoring of molten pool height, area, and temperature in laser metal deposition, *Opt. Laser Technol.* 163 (2024) 109168.
- [7] A. Bandyopadhyay, K.D. Traxel, M. Lang, M. Juhasz, N. Eliaz, S. Bose, Alloy design via Additive Manufacturing: advantages, challenges, applications and perspectives, *Mater. Today* 52 (2022) 207–224.
- [8] S. Chandra, J. Radhakrishnan, S. Huang, S. Wei, U. Ramamurty, Solidification in metal Additive Manufacturing: challenges, solutions, and opportunities, *Prog. Mater. Sci.* 148 (2025) 101361.
- [9] I. Gibson, D.W. Rosen, B. Stucker, *Additive Manufacturing Technologies: Rapid Prototyping to Direct Digital Manufacturing*, Springer, New York, 2010.
- [10] ISO/ASTM 52900:2021(en), Additive Manufacturing—General Principles—Fundamentals and Vocabulary, <https://www.iso.org/obp/ui/#iso:std:iso-astm:52900:ed-2:v1:en> (accessed 20 March 2025).
- [11] K. Wang, Z. Zhang, D. Xiang, J. Ju, Research and progress of laser cladding: process, materials and applications, *Coatings* 12 (2022) 1382.
- [12] X. Zhang, W. Cui, W. Li, F. Liou, A hybrid process integrating reverse engineering, pre-repair processing, Additive Manufacturing, and material testing for component remanufacturing, *Materials* 12 (2019) 1961.
- [13] J.D. Hamilton, D. Trauernicht, D. Cormier, I.V. Rivero, Laser-based directed energy deposition remanufacturing of gray cast iron using stainless steel 316L and Inconel 625 filler materials, *Adv. Eng. Mater.* 25 (2023) 2301212.
- [14] A.R. Bakhtari, H.K. Sezer, O.E. Canyurt, O. Eren, M. Shah, S. Marimuthu, A review on laser beam shaping application in laser-powder bed fusion, *Adv. Eng. Mater.* 26 (2024) 2302013.
- [15] A. Saboori, A. Aversa, G. Marchese, S. Biamino, M. Lombardi, P. Fino, Application of directed energy deposition-based Additive Manufacturing in repair, *Appl. Sci.* 9 (2019) 3316.
- [16] A. Bouabbou, S. Vaudreuil, Understanding laser-metal interaction in selective laser melting Additive Manufacturing through numerical modelling and simulation: a review, *Virtual Phys. Prototyping* 17 (2022) 543–562.
- [17] C. Meier, R.W. Penny, Y. Zou, J.S. Gibbs, A.J. Hart, Thermophysical phenomena in metal Additive Manufacturing by selective laser melting: fundamentals, modeling, simulation, and experimentation, *Annu. Rev. Heat Transf.* 20 (2017) 241–316.
- [18] T. Moges, G. Ameta, P. Witherell, A review of model inaccuracy and parameter uncertainty in laser powder bed fusion models and simulations, *J. Manuf. Sci. Eng.* 141 (2019) 040801.
- [19] A.J. Pinkerton, An analytical model of beam attenuation and powder heating during coaxial laser direct metal deposition, *J. Phys. Appl. Phys.* 40 (2007) 7323–7334. <https://doi.org/10.1088/0022-3727/40/23/012>.
- [20] D. Eisenbarth, P.M. Borges Esteves, F. Wirth, K. Wegener, Spatial powder flow measurement and efficiency prediction for laser direct metal deposition, *Surf. Coat. Technol.* 362 (2019) 397–408. <https://doi.org/10.1016/j.surfcoat.2019.02.009>.

- [21] ISO/ASTM 52900:2015(E), Standard terminology for Additive Manufacturing – general principles – terminology, ASTM International, West Conshohocken, PA, 2015.
- [22] A. Bandyopadhyay, B. Heer, *Addit. Manuf. Technol. Mater. Sci. Eng. R Rep.* 129 (2018) 1–16. <https://doi.org/10.1016/j.mser.2018.04.001>.
- [23] S.M. Thompson, et al., *Addit. Manuf.* 8 (2015) 36–62. <https://doi.org/10.1016/j.addma.2015.07.001>.
- [24] Y. Li, et al., *Acta Biomater.* 77 (2018) 380–393. <https://doi.org/10.1016/j.actbio.2018.07.011>.
- [25] J.M. Wilson, et al., *J. Clean. Prod.* 80 (2014) 170–178. <https://doi.org/10.1016/j.jclepro.2014.05.084>.
- [26] A. Hess, M.F. Zaeh, Online adjustment of the laser beam position in laser metal deposition by means of coaxial process observation, *Phys. Procedia* 83 (2016) 564–573. <https://doi.org/10.1016/j.phpro.2016.08.058>.
- [27] P.A.J. Lusty, N.M. Everitt, J. Allen, W.M. Steen, The influence of laser beam and powder plume alignment on the properties of laser direct metal deposition components, *J. Mater. Process. Technol.* 210 (2010) 2173–2180. <https://doi.org/10.1016/j.jmatprotec.2010.07.020>.
- [28] R. Schmitt, B. Mohr, L. Steinkamp, Optical monitoring systems for process control in laser materials processing, in: *Proc. 19th Congr. Int. Soc. Photogramm. Remote Sens. (ISPRS)*, Amsterdam, 2000.
- [29] D. Schuöcker, *Laser Assisted Fabrication of Materials*, Springer Series in Materials Science, Vol. 107, Springer, Wien/New York, 2006. <https://doi.org/10.1007/978-3-211-29982-7>.